Novel Electrochemical Fingerprinting Methods for Precise Determination of Pt_{Shell} Coverage on Ru_{Core} Nanoparticles

Ehab N. El Sawy, Hany A. El-Sayed, and Viola I. Birss*
Department of Chemistry, University of Calgary, 2500 University Drive N.W.
Calgary, Alberta, Canada T2N 1N4

Supporting Information

S1   Extended Experimental Methods

S1.1   Ru nanoparticle (NP) synthesis

Ru NPs were synthesized using ethylene glycol (EG) as both the solvent and reducing agent, with polyvinyl pyrrolidone (PVP) used as the capping agent. The Ru precursor (0.0784 g = 0.3 mmol of $RuCl_3.3H_2O$) and the PVP (0.0832 g, average molecular weight 40K) were first dissolved in 60 ml of ethylene glycol. The solution was then gradually heated (3 °C/min) to 130 °C, followed by a fast temperature ramp (5-8 °C/min) to 190 °C (boiling). The solution color changed from green to black at 160 °C, indicating the reduction of the Ru salt and the formation of Ru NPs. The solution was then kept under reflux for 2 hours to ensure complete reduction of the Ru precursor to form the Ru NPs, and then the mixture was cooled to room temperature (RT). The Ru NP size was determined using high resolution transmission electron microscopy (HRTEM), giving an average diameter of ~ 2 nm (Fig. S1a) and ~ 3 nm (Fig. S1b) when EG and pentamethylene glycol (PMG) were used as the solvents, respectively.

S1.2   Ru_{core}@Pt_{shell} nanoparticle synthesis

Ru_{core}@Pt_{shell} nanoparticles (NPs), with a range of Pt shell coverages ranging from 0 to 2 MLs, were synthesized by the addition of an exact number of moles of Pt precursor (*X* g

$H_2PtCl_6.6H_2O$ + 10 ml ethylene glycol (EG) to a controlled volume and concentration of the Ru NP colloidal solution (Section S1.1.1). EG was found to be very suitable as both the solvent and reducing agent, as in the case of Ru NP synthesis. Since the amount of Ru in each synthesis was kept constant (0.0786 g = 0.3 mmol), the desired Ru:Pt ratio, and hence the desired surface coverage of Pt, was obtained by controlling the amount of Pt precursor ($H_2PtCl_6.6H_2O$) added to the Ru colloid-containing solution, assuming that all of the Pt precursor will be reduced to Pt metal.

Once the Pt precursor was homogenously mixed into the Ru colloid, the temperature was then gradually increased to 110 °C (slightly lower than the reduction temperature of the Pt precursor (130 °C when using EG[1])), followed by a fast temperature ramp to 185 °C (boiling). The solution temperature was then kept at 185 °C for 2 hours to prevent the dissolution of the Ru core by galvanic coupling with Pt[2], and also to ensure the complete reduction of the Pt precursor. Note that the reduction temperature of the Pt and Ru precursors used in this study is 130 and 160 °C, respectively.

To better understand the relationship between the Pt salt concentration employed and the expected number of Pt MLs deposited around the Ru core NPs, the following analysis is given. To start, the number of moles (n) in a NP depends on its volume ($4/3\pi r^3$, assuming that the NPs are spherical in shape), density (ρ), and molar mass (M), as shown in equation 1.

$$n\,(mole) = \frac{\rho\,(g\,cm^{-3}) \times {}^4\!/_3\pi r^3 (g\,cm^{-3})}{M\,(g\,mole^{-1})}$$

In the case of the core@shell NPs prepared in the presence of capping agents, such as PVP, the shell is known to grow smoothly around the core particle surface structure [3-5]. Thus, the addition of one monolayer (ML) coverage to a single NP will result in an increase in the NP diameter (volume) by ~ 0.5 nm in the case of Pt or Ru (2× Pt or Ru atom diameter, which is 0.272 or 0.268 nm, respectively). The corresponding increase in the number of moles of Pt, per Ru nanoparticle, can then be calculated using equation (1). As Pt and Ru have a similar density, ρ/M value, (0.11 and 0.12 mol cm^{-3}, respectively), for simplicity, we assume that the number of moles in the $Ru_{core}@Pt_{shell}$ NPs is the same as what would be found in a Ru NP with a similar diameter.

In the case of the Ru_{core} NPs formed using ethylene glycol (EG) and having a diameter of 2 nm, using this approach, we found that Ru:Pt molar ratios of 1:1 and 1:2.4 are necessary to form one and two monolayers of Pt_{shell} on a Ru_{core} NP, respectively, as illustrated in Fig. S2a. However, in the case of Ru_{core} (PMG) nanoparticles with a diameter of 3 nm, Fig. S2b shows that Ru:Pt molar ratios of 1:0.6 or 1:1.4 are necessary to deposit one or two monolayers of Pt_{shell}, respectively.

S*1.3*   *Characterization of Ru$_{core}$ and Ru$_{core}$@Pt$_{shell}$ NPs*

High resolution transmission electron microscopy (HRTEM), coupled with energy dispersive X-ray spectroscopy (EDS) (Tecnai F20 G2 FEG-TEM, Microscopy and Imaging Facility (MIF), University of Calgary, Alberta, Canada), was used to confirm the formation of the core@shell NP structure and to determine the size of the $Ru_{core}@Pt_{shell}$ NPs. The TEM samples were prepared by diluting the NP colloidal solutions with ethanol, and then a drop of the

diluted solution was placed on one side of a TEM grid (Lacey Carbon or Cu-carbon coated TEM grid).

The $Ru_{core}@Pt_{shell}$ NPs were also produced in the form of a fine powder in order to determine their composition (in atomic % of each of Ru and Pt) and crystal structure. Therefore, several cycles of NP isolation (centrifugation) and washing (acetone) were performed. The precipitate was then dried under vacuum at room temperature and ground to a fine powder. Wavelength Dispersive X-ray Spectroscopy (WDS) was used (JEOL JXA- 8200 electron microprobe, The University of Calgary Laboratory for Electron Microprobe Analysis (UCLEMA), Alberta, Canada) for the determination of the $Ru_{core}@Pt_{shell}$ NP composition. Also, Powder X-ray Diffraction (PXRD) (Rigaku Multiflex X-ray Diffractometer, Department of Geosciences, University of Calgary, Alberta, Canada), with CuK_α radiation ($\lambda = 1.5406$ nm, V = 40 kV, and I = 20 mA), was used to determine the NP crystal structure.

S1.4 Electrochemical studies

For electrochemical evaluation, the $Ru_{core}@Pt_{shell}$ NPs were loaded on Vulcan Carbon (VC), with a NP:VC mass ratio of 1:9, by adding the colloidal Ru solution to a homogenously mixed VC/ethanol solution, followed by stirring for 2-4 hours. After several cycles of powder collection (centrifuging) and washing with acetone, the $Ru_{core}@Pt_{shell}$/VC material was dried under vacuum at room temperature. Thermogravimetric Analysis (TGA-Mettler-Toledo StarE) was performed in air from room temperature to 1000 °C, using a ramp rate of 10 °C/min, in order to accurately determine the $Ru_{core}@Pt_{shell}$ NP loading on VC.

Standard three-electrode circuitry, using an EG&G PARC 173 potentiostat combined with a PARC 175 function generator, was employed for all of the electrochemical measurements. Data were collected using PowerLab/400 and plotted with Chart for Windows v5. In this work, a two-compartment glass cell was used, where the working and counter electrodes were placed in the main compartment and the reference electrode was in the second compartment, connected to the main compartment through a Luggin capillary.

The working electrode (WE) consisted of a 7 mm diameter glassy carbon (GC) rod, embedded in a Teflon holder and covered with a thin film of the NP/VC mixture. This was prepared, as an ink, by mixing 0.3 ml of a 1% w/w Nafion solution, 0.6 ml of isopropanol, 0.1 ml of water, and 10 mg of the $Ru_{core}@Pt_{shell}$ NP/VC powder, followed by sonication for $\geq$ 30 min. Ca. 20 µl of the $Ru_{core}@Pt_{shell}$ NP/VC ink was deposited onto the WE (GC) surface via a 2-20 µl micropipette, then allowing it to dry at room temperature. The counter electrode (CE) consisted of a platinized Pt gauze, while the reference electrode (RE) was a reversible hydrogen electrode (RHE), to which all potentials are referred in this work. All solutions were prepared using Analar-Grade chemicals and triply distilled water. The solutions were thoroughly deaerated by bubbling N_2 gas through the solution for 15 min prior to each experiment. All measurements were carried out at room temperature ($22 \pm 1^{o}C$).
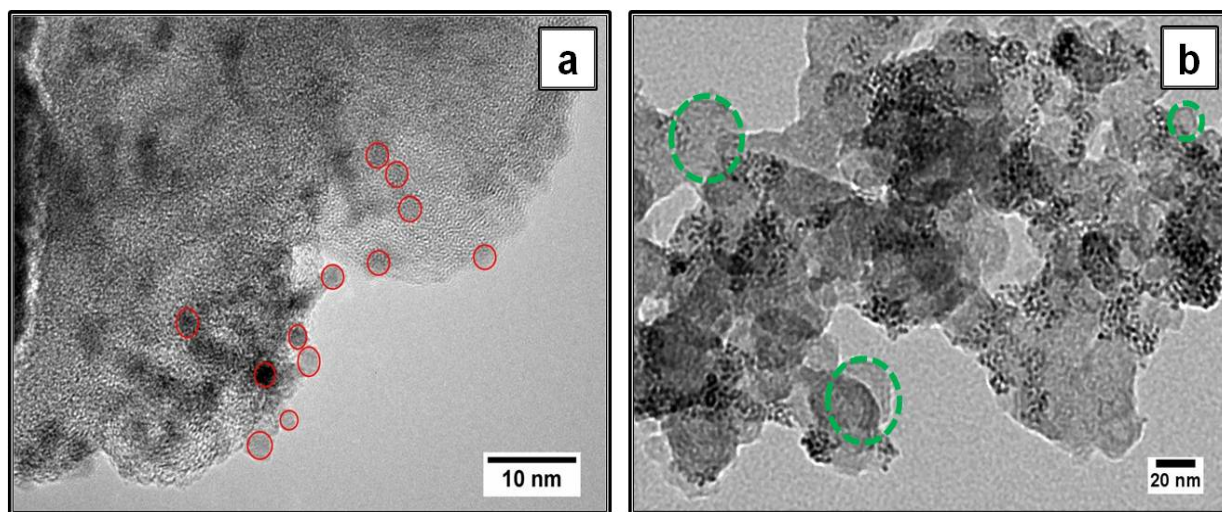
Figure S1: TEM bright field images of (a) Ru (EG) NPs, highlighted by the solid red circles, deposited on a Lacy Carbon-coated Ni TEM grid, and (b) Ru (PMG) NPs on VC (highlighted by the dashed green circles), deposited on a carbon-coated 400 mesh Cu TEM grid.

Fig. S1a shows a high resolution transmission electron microscopy (HRTEM) image of Ru NPs dispersed on Lacey Carbon TEM grids (Electron Microscopy). The average Ru NP size was determined using ImageJ to be ~ 2 nm, which matches the characteristics of Ru NPs prepared by other groups using the same method [5]. In the case of the $Ru_{core}@Pt_{shell}$ (PMG) NPs, the Ru_{core} NP size is ~ 3 nm (Fig. S1b). The NPs were loaded on a Vulcan carbon (VC) support with an average particle size in the range of 20-50 nm, as shown in Fig. S1b and also reported previously by others [6]. The VC particles are highlighted by the dashed green circles in Fig. S1b.
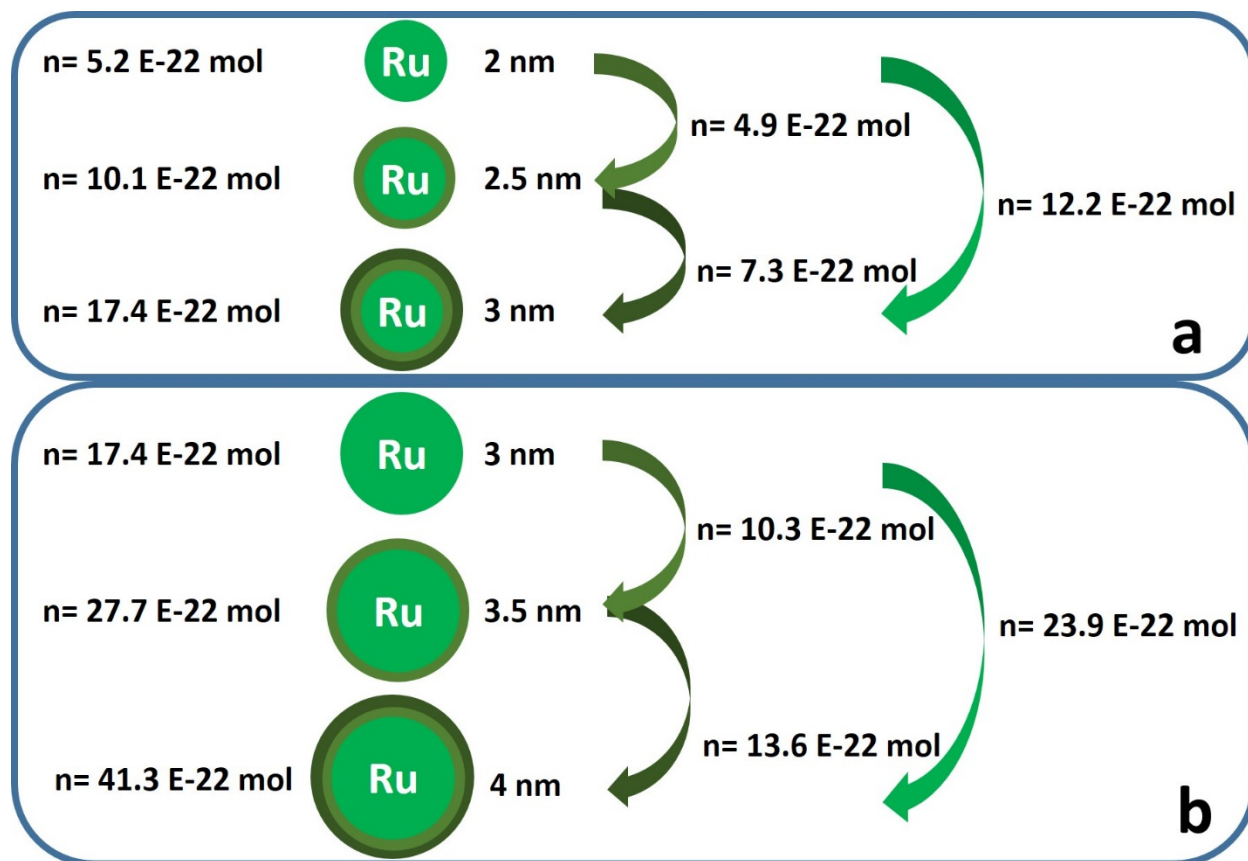
Figure S2: Schematic diagram showing the calculated number of moles, obtained using equation (1), in each $Ru_{core}@Pt_{shell}$ NP before and after the addition of one and two monolayers of $Pt_{shell,}$ in the case of Ru_{core} NPs (a) 2 nm and (b) 3 nm in diameter.
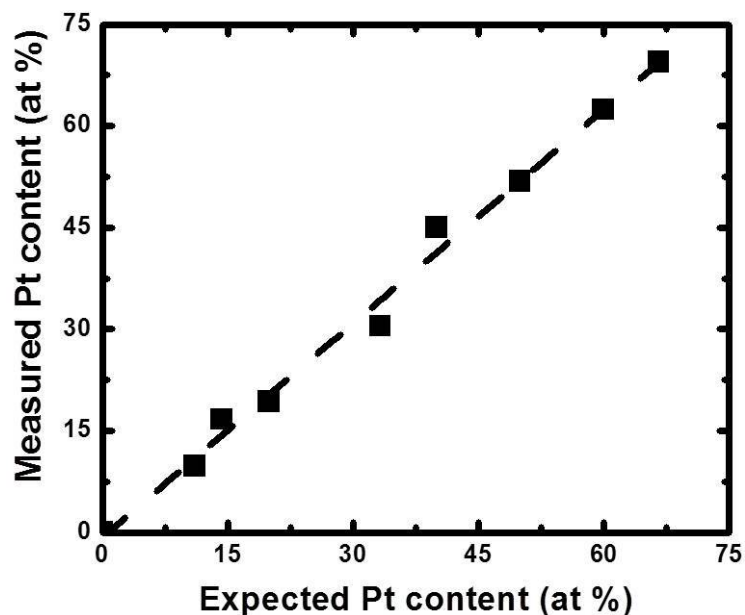
Figure S3: Relationship between the expected Pt content (based on the synthesis solution composition) and the experimentally measured Pt content (based on WDS measurements) of $Ru_{core}@Pt_{shell}$ NPs (2 nm Ru NP core).

Fig. S3 shows a linear relationship (with a slope of one) between the expected Pt content (at %) in the $Ru_{core}@Pt_{shell}$ NPs (2 nm Ru core), based on the composition of the synthesis solution, and the real Pt content (at %), obtained using wavelength dispersive X-ray spectroscopy (WDS). This shows that the Pt content of the NPs, and hence the Pt shell coverage, can be fully controlled simply by changing the synthesis solution composition (Ru NPs and $H_2PtCl_6.6H_2O$).
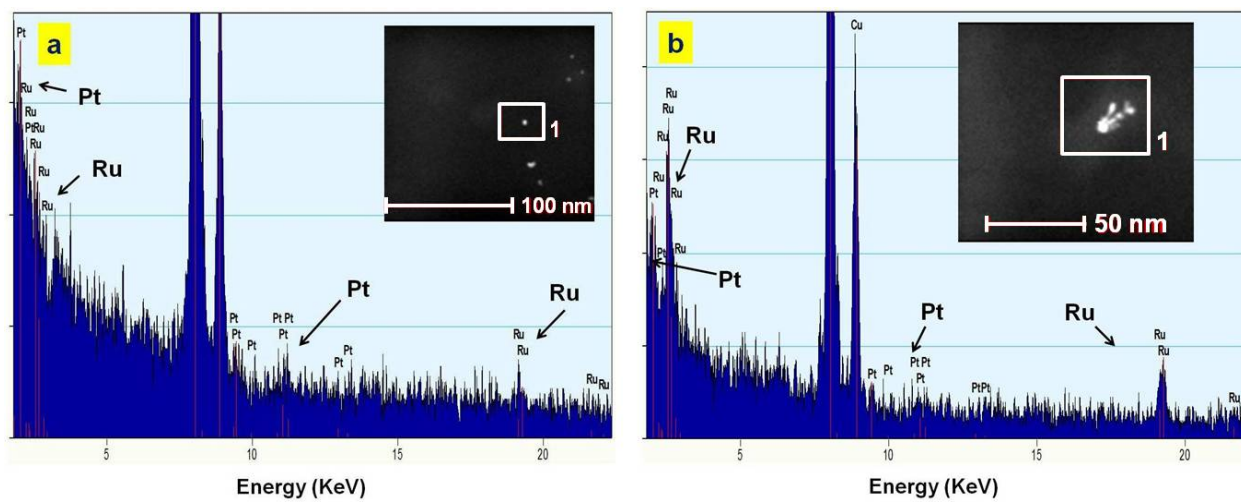
Figure S4: EDX spectra of $Ru_{70}@Pt_{30}$ NPs (Ru core diameter = 2 nm) on a carbon-coated Cu TEM grid, for (a) a single NP and (b) a cluster of NPs. Insets: Dark field TEM images, showing the area that was used to collect the EDX spectra.

Transmission electron microscopy (TEM), coupled with energy dispersive X-ray analysis (EDX), was used to confirm the formation of $Ru_{core}@Pt_{shell}$ NPs, as opposed to individual Ru and Pt NPs. Fig. S4a shows the EDX spectrum of a single NP, expected to be $Ru_{70}@Pt_{30}$, based on WDS measurements, while Fig. S4b shows the spectrum of a cluster of NPs. Both Pt and Ru are seen to be present in the single NP in Fig. S4a, while in Fig. S4b, the signal intensities for Pt and Ru are both higher, as expected for a cluster of $Ru_{core}@Pt_{shell}$ NPs.
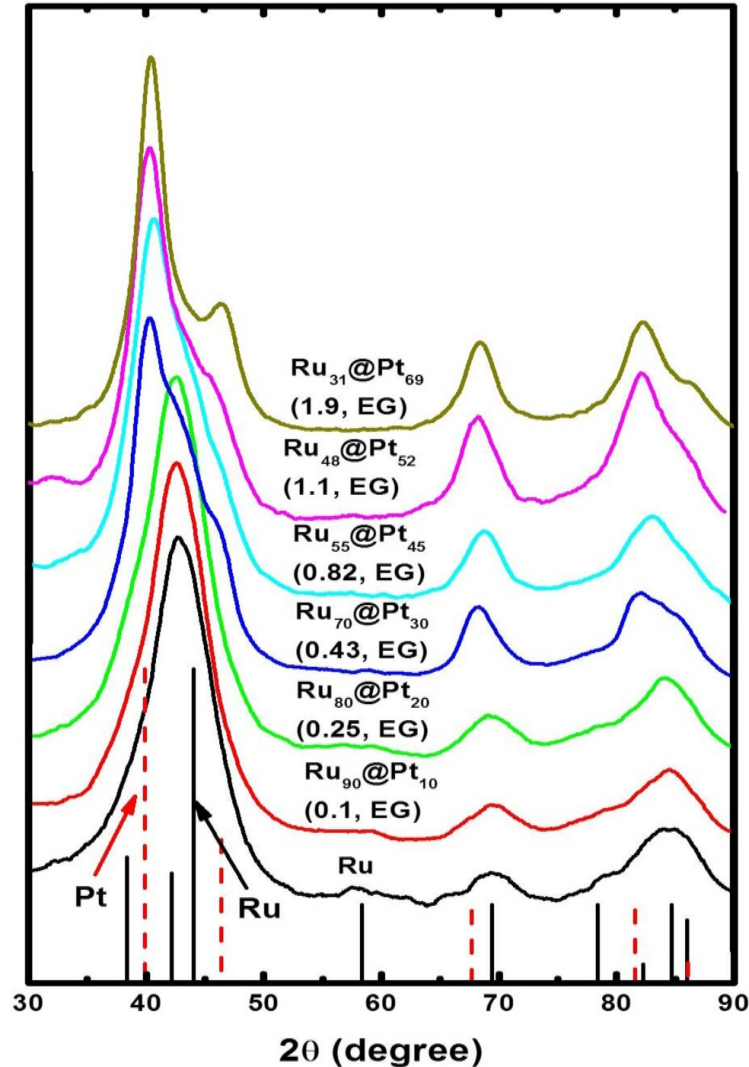
Figure S5: Powder XRD patterns of $Ru_{core}@Pt_{shell}$ (EG, 2 nm dia Ru core) NPs in the 2θ range of $30°-90°$. The Pt_{shell} coverage of the $Ru_{core}@Pt_{shell}$ NPs is indicated in brackets in number of monolayers, along with the solvent used in the synthesis, ethylene glycol (EG). The solid and dashed vertical lines represent the 2θ values of the Ru HCP (PDF#06-0663) and Pt FCC (PDF#87-640), respectively.

In order to monitor the changes in the Ru@Pt NP crystal structure as the Pt_{shell} coverage was controllably increased, Powder X-ray Diffraction (PXRD) was employed. X-ray diffraction from thin films is rarely observed, as there is insufficient scattering matter present compared to the sample bulk [7]. However, NPs provide a very high density of scattering matter, which

enhances the XRD signal relative to thin film samples [4, 7]. Therefore, changes in the $Ru_{core}@Pt_{shell}$ crystal structure due to changes in the shell layer can be monitored using PXRD [4].

Fig. S5 shows the XRD patterns of a series of Ru_{core} and $Ru_{core}@Pt_{shell}$ NPs with varying Pt coverage (indicated in number of monolayers, in brackets, along with the solvent used in their synthesis, ethylene glycol (EG)). Theoretically, the main Ru XRD peak (101) appears at 44.01°, while the main Pt peak (111) appears at 39.89°, indicating that the interatomic distance is larger for Pt than for Ru.

In the case of the pure Ru NPs, the XRD pattern shows an overlap between the peaks for the (100) plane (at 38.39°), the (002) plane (at 42.15°), and the (101) plane (at 44.01°), due to the broadening of the main peak (101). The broadening of the main peak (101) could result from the small size of the Ru NPs or may indicate that the Ru NPs consist of still smaller crystallites. S. Alayoglu et al [4] indicated that Ru NPs (3 nm in diameter), prepared using the same method as employed here and examined using EXAFS, TEM and XRD methods consist of still smaller crystallites.

In the case of the $Ru_{core}@Pt_{shell}$ NPs, when the Ru_{core} is covered with a sub-monolayer of Pt, no changes in the Ru (101) peak are observed up to a Pt coverage of 0.25 ML ($Ru_{80}@Pt_{20}$), as seen in Fig. S5. At a Pt coverage of 0.43 ($Ru_{70}@Pt_{30}$), the Pt (111) and (200) XRD peaks appear in combination, with a distinguishable shoulder, likely related to the Ru (101) peak. With a further increase in the Pt coverage up to 1.9 monolayers, the Ru (101) peak gradually decreases in size until it totally disappears, as can be seen in the case of the $Ru_{31}@Pt_{69}$ (1.9) NPs (Fig. S5). The XRD pattern of the Ru core shows that it has a disordered structure, as has been reported by others[4]. However, the addition of a Pt shell, which is more crystalline than the Ru core[4], has the

ability to force the Ru core to be more ordered. Therefore, these gradual changes (Fig. S5) in the XRD patterns of the $Ru_{core}@Pt_{shell}$ NPs, moving from Ru to Pt, indicate the gradual expansion of the Ru_{core} lattice as the Pt_{shell} coverage increases [8], also confirming the formation of $Ru_{core}@Pt_{shell}$ NPs rather than individual Ru and Pt NPs [4].

In order to further verify that the XRD pattern in Fig. S5 is due to the crystal structure of the $Ru_{core}@Pt_{shell}$ NP as a whole and not due to the Ru core or the Pt shell alone, the XRD pattern of the $Ru_{31}@Pt_{69}$ (1.9, EG) NPs was quantitatively analyzed. From the TEM analysis, the Ru core is shown to have a particle size of ca. 2 nm. Therefore, the addition of 2 MLs of Pt in the shell layer is expected to increase the particle size to 3.1 nm (0.55 nm for each Pt ML). Using the Scherrer equation[9], the particle size (crystallite size) was found to be 3.2 ± 0.1 nm, which is very close to this predicted $Ru_{core}@Pt_{shell}$ particle size, adding further evidence of core@shell structure formation. Also, the shift of the (111) peak position from 39.9° for bulk Pt to 40.5° (Fig. S5) is an indication of the compression of the Pt shell, as expected for a Ru@Pt core@shell structure[4].
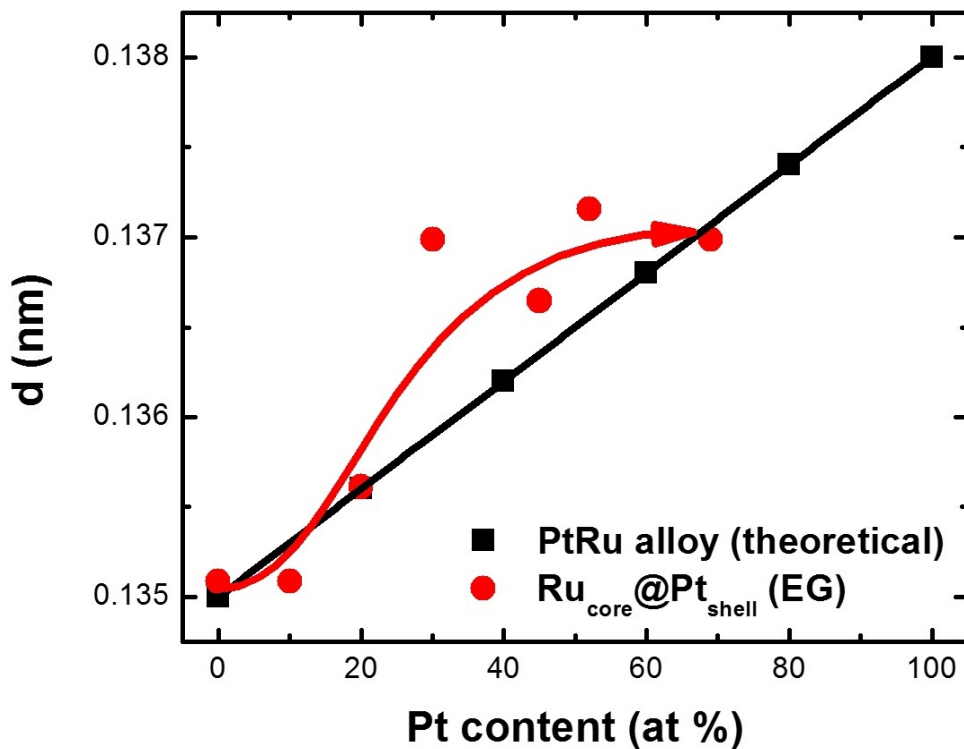
Figure S6: Comparison between the change in d-spacing for the PtRu alloy (theoretical calculation) and that obtained for the Ru$_{core}$@Pt$_{shell}$ NPs (EG) by XRD analysis, both as a function of Pt content. The d-spacing was calculated using the (110) and (220) peak positions for Ru and Pt, respectively.

The Ru (110) and Pt (220) XRD peaks at 69.4° and 67.7°, respectively, are the only peaks that do not overlap with any other Ru or Pt XRD peaks. Therefore, tracking the peak position change, which moves from the Ru value to that of Pt with increasing Pt content, could differentiate between alloy and core@shell NP formation. Fig. S6 shows the predicted d-spacing of a Pt-Ru alloy with different Pt contents in comparison to what was obtained in the case of the Ru$_{core}$@Pt$_{shell}$ (EG) NPs. The d-spacing was calculated based on the XRD peak at 68.3°-69.5°, which is correlated with the Ru (110) and Pt (220) peaks, using Braggs law[10].

Fig. S6 shows that, in the case of the Pt-Ru alloy, the d-spacing should increase linearly with increasing Pt content. However, in the case of the Ru$_{core}$@Pt$_{shell}$ (EG) NPs, the d-spacing

changed dramatically with increasing Pt content, from 10 to 30 at % (0.1 to 0.43 ML of Pt_{shell}), before reaching a steady-state at a Pt content of 30-70 at % (0.43-1.9 ML Pt_{shell}). The difference between the expected d-spacing of a Pt-Ru alloy and that obtained in the case of the $Ru_{core}@Pt_{shell}$ NPs, investigated here is further proof of the formation of the core@shell structure. This is also associated with a slight compression of the Pt shell (0.43-1.9 ML) and an expansion and rearrangement of the Ru core structure.
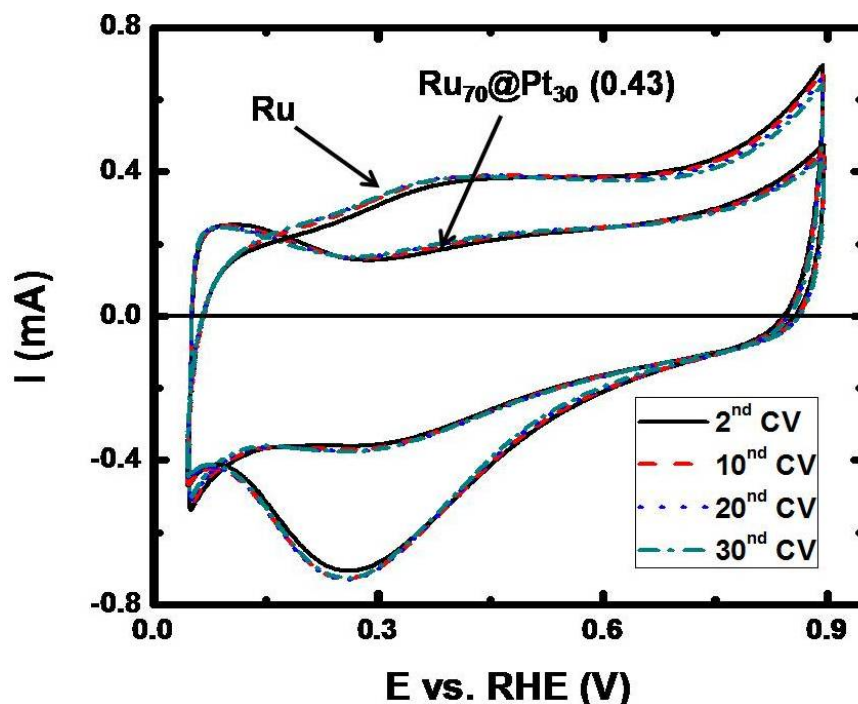
Figure S7: Cyclic voltammetry (20 mV/sec) of Ru NPs and $Ru_{70}@Pt_{30}$ (0.43) NPs, supported on Vulcan Carbon, in RT 0.5 M H_2SO_4, showing no change in the CV responses after many successive CV scans.

In this study, the peak current (i_{peak}) of the Ru oxide reduction peak, centred at 0.25-0.35 V vs. RHE [11], has been used to track the exposed fraction of the Ru_{core} surface. Fig. S7 confirms that the CV response is independent of CV cycling time, at least for 30 successive cycles, revealing the very good stability of the nanoparticle surface structure, as well as the lack of NP agglomeration. These changes would have been seen by a gradually decreasing CV signal with time of cycling.

The presence of Pt as a sub-shell on the surface of the Ru core, rather than being physically mixed or alloyed with Ru, may explain the difference between our work and the findings reported in the work of Ochal et al[5]. Also, the higher upper potential and slower scan rate used in this former work[5] (1.0 V and 10 mV/sec, respectively) may have enhanced the dissolution of Ru relative to what we are observing.
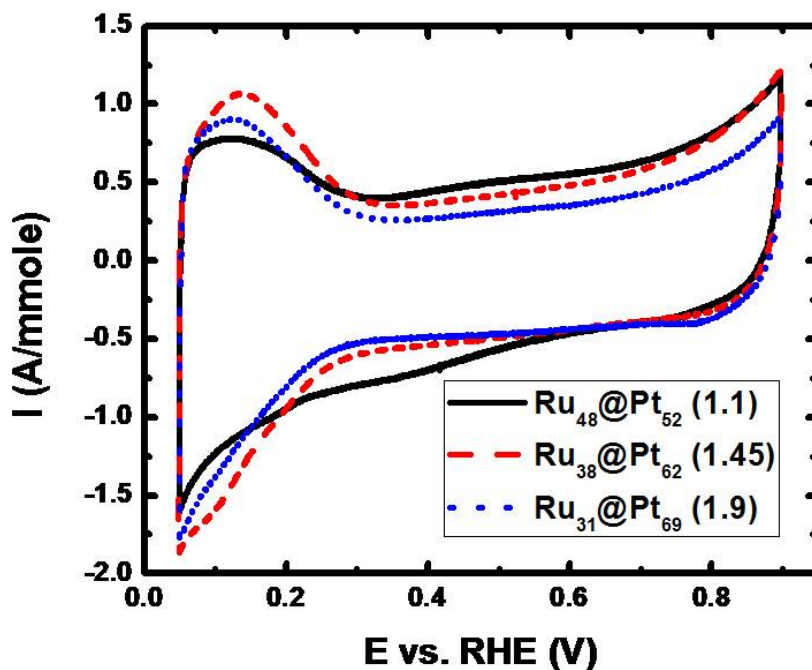
Figure S8: Cyclic voltammetry (20 mV/sec) of $Ru_{38}@Pt_{62}$ (1.45) and $Ru_{31}@Pt_{69}$ (1.9) NPs, supported on Vulcan Carbon powder, in RT 0.5 M H_2SO_4.

The electrochemical behavior of $Ru_{48}@Pt_{52}$ (1.1), $Ru_{38}@Pt_{62}$ (1.45), and $Ru_{31}@Pt_{69}$ (1.9) NPs when the potential was cycled between 0.05 and 0.9 V vs. RHE in deaerated 0.5 M H_2SO_4 at room temperature is shown in Fig. S8. In the case of $Ru_{48}@Pt_{52}$ (1.1), a very small RuOx peak is seen, which is explained by the exposure of a small amount of Ru at imperfections in the first Pt_{shell} monolayer. These imperfections disappear at higher Pt_{shell} coverages (1.45 and 1.9 MLs), as indicated by the absence of this RuOx peak for Pt_{shell} coverage of 1.45 and 1.9.
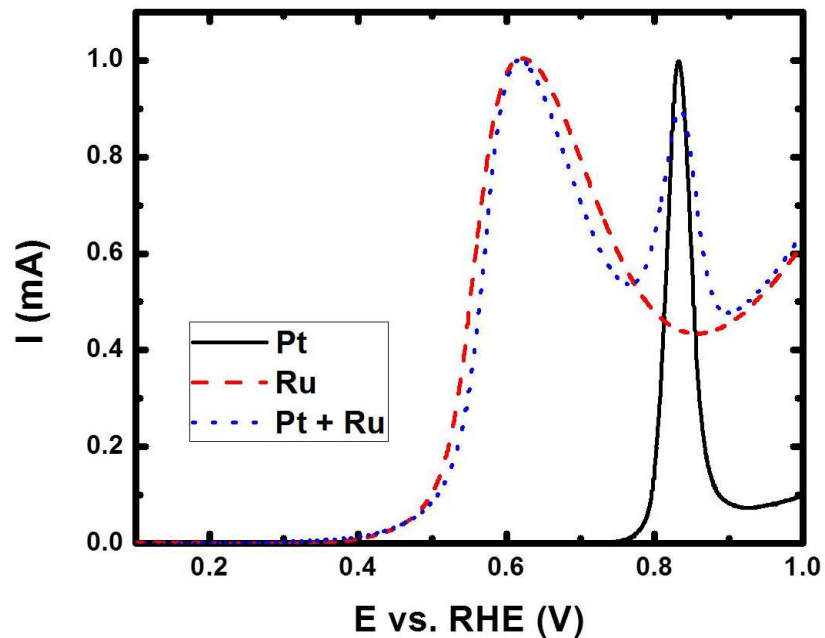
Figure S9: CO stripping voltammetry (20 mV/sec) at Pt, Ru, and physically mixed Pt+Ru (1:1 mass ratio) nanoparticles, all supported on Vulcan Carbon powder, in RT 0.5 M H_2SO_4. CO was pre-adsorbed at 0.05 V for 15 min and the CO stripping currents were normalized to the higher of the two current peaks for easier comparison of the peak potentials.

The CO stripping response for the Ru/VC, Pt/VC, and physically mixed Pt/VC + Ru/VC catalysts is shown in Fig. S9. In all cases, only very small currents are observed at potentials negative of the CO stripping peak, which indicates full coverage of the catalyst surfaces by CO. The Ru/VC and Pt/VC CO stripping peaks appear at 0.62 and 0.83 V vs. RHE, respectively, matching closely with literature values [5, 12, 13]. Two CO stripping peaks, reflecting CO stripping from each of the Ru and Pt sites, are observed when the Pt and Ru NPs are physically mixed together. This indicates the absence of any effect of the Ru and Pt NPs on each other in terms of their catalytic activities towards CO oxidation.
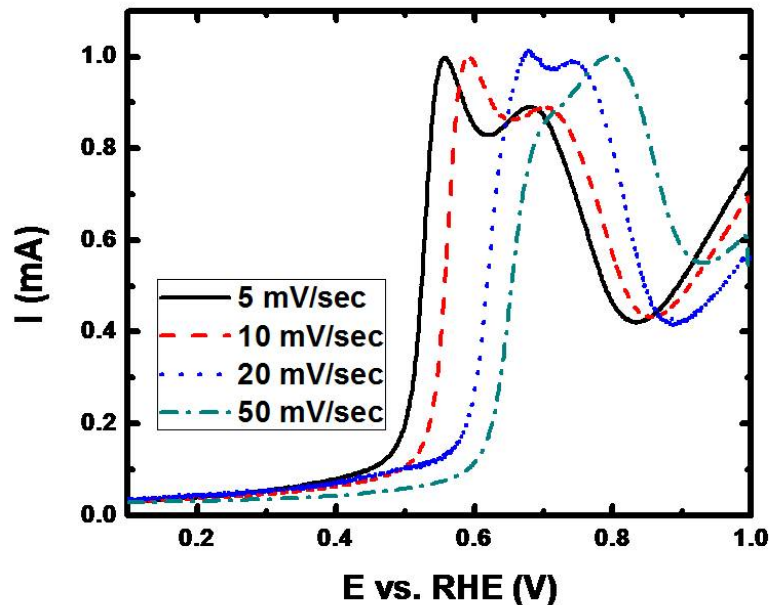
Figure S10: CO stripping voltammetry at scan rates of 5-50 mV/sec for $Ru_{38}@Pt_{62}$ (1.45)/VC in RT 0.5 M H_2SO_4. CO was pre-adsorbed at 0.05 V for 15 min and the current was then normalized to the higher of the two current peaks for easier comparison of the CO stripping peak potentials.

The CO stripping voltammetry of $Ru_{38}@Pt_{62}$ (1.45)/VC at different scan rates reveals two peaks (Fig. S10), which are related to Type A and Type B surface Pt atoms (Fig. 2). These two peaks are well defined and are seen clearly at low scan rates (5 and 10 mV/sec), while they overlap slightly at a scan rate of 20 mV/sec and become ill-defined at still higher scan rates (50 mV/sec). Also, the CO stripping peak and onset potentials shift towards more positive values as the scan rate increases. This phenomenon is well known for CO stripping at Pt electrodes [14-16].
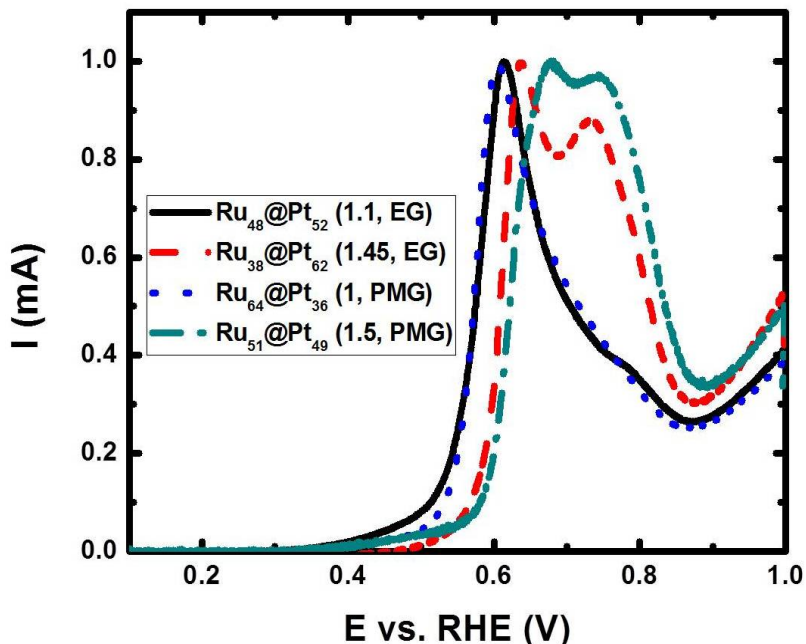
Figure S11: CO stripping voltammetry (20 mV/sec) for $Ru_{core}@Pt_{shell}$/VC NPs in RT 0.5 M H_2SO_4. CO was pre-adsorbed at 0.05 V for 15 min and the current during CO stripping was then normalized to the higher of the two current peaks for easier comparison of the peak potentials. The Pt shell coverage of the Ru core and the synthesis solvent (EG = ethylene glycol and PMG = pentamethylene glycol) are indicated in brackets.

The CO stripping voltammetry of $Ru_{core}@Pt_{shell}$/VC NPs, prepared using either ethylene glycol or pentamethylene glycol as the solvent and reducing agent, is shown in Fig. S11. A similar CV response is seen in both cases for the same Pt shell coverage, showing that the electrochemical fingerprint of the second Pt monolayer in the Pt shell is independent of the Ru core size.

S3   References

1.   E. N. El Sawy, in *Chemistry*, University of Calgary, Canada, 2013, p. 227.
2.   E. Antolini, *Journal of Solid State Electrochemistry*, 2011, **15**, 455-472.
3.   N. Toshima and T. Yonezawa, *New Journal of Chemistry*, 1998, **22**, 1179-1201.
4.   S. Alayoglu, P. Zavalij, B. Eichhorn, Q. Wang, A. I. Frenkel and P. Chupas, *ACS Nano*, 2009, **3**, 3127-3137.
5.   P. Ochal, J. L. Gomez de la Fuente, M. Tsypkin, F. Seland, S. Sunde, N. Muthuswamy, M. Ronning, D. Chen, S. Garcia, S. Alayoglu and B. Eichhorn, *J. Electroanal. Chem.*, 2011, **655**, 140-146.
6.   W. X. Chen, J. Y. Lee and Z. Liu, *Chemical Communications*, 2002, **0**, 2588-2589.
7.   S. Alayoglu, A. U. Nilekar, M. Mavrikakis and B. Eichhorn, *Nat Mater*, 2008, **7**, 333-338.
8.   A. Schlapka, M. Lischka, A. Gross, U. Kasberger and P. Jakob, *Phys. Rev. Lett.*, 2003, **91**, 016101.
9.   D. W. H. Banham, in *ProQuest Dissertations and Theses*, University of Calgary (Canada), Canada, 2012, p. 238.
10.   J. William D. Casllister, *Materials Science and Engineering: An Introduction*, John Wiley & Sons, Inc., 2004.
11.   S. Hadzi-Jordanov, H. Angerstein-Kozlowska, M. Vukovic◻ and B. E. Conway, *Journal of The Electrochemical Society*, 1978, **125**, 1471-1480.
12.   J. Solla-Gullon, F. J. Vidal-Iglesias, V. Montiel and A. Aldaz, *Electrochimica Acta*, 2004, **49**, 5079-5088.
13.   D. Bokach, J. L. G. de la Fuente, M. Tsypkin, P. Ochal, I. C. Endsjø, R. Tunold, S. Sunde and F. Seland, *Fuel Cells*, 2011, **11**, 735-744.
14.   F. Maillard, E. R. Savinova and U. Stimming, *J. Electroanal. Chem.*, 2007, **599**, 221-232.
15.   K. C. Chou, N. M. Markovic, J. Kim, P. N. Ross and G. A. Somorjai, *The Journal of Physical Chemistry B*, 2003, **107**, 1840-1844.
16.   A. Couto, M. C. Perez, A. Rincon and C. Gutierrez, *The Journal of Physical Chemistry*, 1996, **100**, 19538-19544.